

RevaMp3D: Architecting the Processor Core and Cache Hierarchy for Systems with Monolithically-Integrated Logic and Memory

NIKA MANSOURI GHIASI, MOHAMMAD SADROSADATI, GERALDO F. OLIVEIRA, and
 KONSTANTINOS KANELLOPOULOS, ETH Zurich, Switzerland
 RACHATA AUSAVARUNGNIRUN, MangoBoost, USA
 JUAN GÓMEZ LUNA, JOÃO FERREIRA, and JEREMIE S. KIM, ETH Zurich, Switzerland
 CHRISTINA GIANNOULA, University of Toronto and ETH Zurich, Canada and Switzerland
 NANDITA VIJAYKUMAR, University of Toronto, Canada
 JISUNG PARK, POSTECH, South Korea
 ONUR MUTLU, ETH Zurich, Switzerland

Recent nano-technological advances enable the *Monolithic 3D (M3D)* integration of multiple memory and logic layers *in a single chip*. Such integration enables high-bandwidth connections between layers, which significantly alleviates main memory bottlenecks. We show for a variety of workloads, on a state-of-the-art M3D-based system, that the performance and energy bottlenecks shift from main memory to the processor core and cache hierarchy. Therefore, to effectively utilize the chip’s area, given the applications’ shifted requirements, there is a need to revisit current processor core and cache hierarchy designs that have been conventionally tailored to tackle the memory bottleneck. Based on the insights from our design space exploration, we propose **RevaMp3D**, which introduces five key changes to the state-of-the-art M3D-based system. First, we propose removing the shared last-level cache, based on our observation that doing so achieves speedups on par with, or even exceeding, speedups achieved by increasing its size or reducing its latency, across all our workloads. Second, since our analysis shows that improving L1 cache latency has a large impact on performance in M3D, we reduce L1 cache latency by leveraging an M3D layout that reduces its wire lengths. Third, we leverage the area reclaimed from removing large caches to widen and scale up various structures in the processor pipeline that enable greater instruction-level parallelism. To avoid latency penalties from these larger structures, we leverage M3D layouts that keep their wire lengths short. Fourth, to facilitate high thread-level parallelism, we propose a new fine-grained synchronization technique, using M3D’s dense inter-layer connectivity. Fifth, we leverage the M3D main memory to mitigate the performance and energy bottlenecks of the processor core. To this end, we propose a processor frontend design that memoizes the repetitive fetched, decoded, and reordered instructions, stores them in main memory at low cost, and turns off the relevant parts of the core when possible. The high-bandwidth, energy-efficient M3D memory enables storing and loading the memorized instructions efficiently, eliminating the need for large SRAM for storing the instructions. Our evaluation using a wide range of 20 real-world workloads and 7 multi-programmed mixes shows that RevaMp3D provides $1.2\times$ – $2.9\times$ speedup and $1.2\times$ – $1.4\times$ energy reduction, while achieving 12.3% smaller area, compared to the state-of-the-art M3D-based system. We also analyze the impact of RevaMp3D’s design decisions for M3D systems with various main memory latency values since latency can vary depending on the design decisions made to meet certain requirements of the target system. This analysis facilitates making the appropriate design decisions based on latency, thereby benefiting a wide range of workloads.

CCS Concepts: • **Computer systems organization** → **Architectures**; • **Hardware** → **Analysis and design of emerging devices and systems**.

Permission to make digital or hard copies of all or part of this work for personal or classroom use is granted without fee provided that copies are not made or distributed for profit or commercial advantage and that copies bear this notice and the full citation on the first page. Copyrights for components of this work owned by others than the author(s) must be honored. Abstracting with credit is permitted. To copy otherwise, or republish, to post on servers or to redistribute to lists, requires prior specific permission and/or a fee. Request permissions from permissions@acm.org.

© 2018 Copyright held by the owner/author(s). Publication rights licensed to ACM.

Manuscript submitted to ACM

Manuscript submitted to ACM

1

Additional Key Words and Phrases: Monolithic 3D Integration, Memory Bottlenecks, Processor Core, Cache Hierarchy

ACM Reference Format:

Nika Mansouri Ghiasi, Mohammad Sadrosadati, Geraldo F. Oliveira, Konstantinos Kanellopoulos, Rachata Ausavarungnirun, Juan Gómez Luna, João Ferreira, Jeremie S. Kim, Christina Giannoula, Nandita Vijaykumar, Jisung Park, and Onur Mutlu. 2018. RevaMp3D: Architecting the Processor Core and Cache Hierarchy for Systems with Monolithically-Integrated Logic and Memory. In *Proceedings of Make sure to enter the correct conference title from your rights confirmation email (Conference acronym 'XX)*. ACM, New York, NY, USA, 26 pages. <https://doi.org/XXXXXXXX.XXXXXXX>

1 Introduction

Recent nano-technological advances enable the *Monolithic 3D (M3D)* integration of multiple logic and memory layers on a single chip [1–11]. M3D integration is a promising technology to alleviate the memory bottleneck that significantly limits the performance and energy efficiency of data-intensive applications in conventional systems. M3D integration enables significantly higher main memory bandwidth compared to other 3D integration technologies, such as Through Silicon Via (TSV)-based [8, 12–14] or hybrid bonding-based [15–20] integrations. This is due to M3D’s much higher density of Inter-Layer Vias (ILVs) that connect different device layers. M3D integration can also lead to lower main memory latency by exploiting the fine-grained ILVs to efficiently enable (i) a large number of memory channels, each connected to relatively small memory arrays with shorter wire lengths, (ii) fine-grained 3D layout of the memory array to further shorten the wires, and (iii) low-latency interconnections between logic and memory layers on the same chip.

Due to its benefits, M3D integration has received substantial interest in both academia (e.g., [1–11, 21–27]) and industry (e.g., [28–33]). Several prior works propose improvements for M3D-based systems, mainly focusing on three aspects. First, at the device and circuit levels, various works (e.g., [3, 10, 34–49]) propose improvements to the logic and memory components and their integration in M3D substrates. Second, at the architecture level, some works (e.g., [14, 50–56]) demonstrate the impact of the M3D integration of logic layers on the performance and energy efficiency of logic components, such as SRAM structures in processor cores and networks on chips. Other works (e.g., [10, 52]) explore the memory system challenges in M3D (e.g., designing main memory array structures and controllers). Third, at the application level, various works (e.g., [51, 57–63]) propose application-specific M3D accelerators.

While prior works propose various improvements for M3D-based systems, no prior work re-examines the processor core and cache hierarchy designs based on the requirements of real-world applications on systems with monolithically-integrated logic and memory. Therefore, to effectively leverage M3D integration’s benefits, it is important to understand its implications on the performance and energy bottlenecks of real-world applications. These implications can then guide re-examining processor core and cache hierarchy designs. Based on our experimental analysis of a variety of workloads simulated on a state-of-the-art M3D-based system [5, 7–9], we make two key observations. First, compared to the 2D and 3D systems, performance bottlenecks in the M3D-based system *shift* substantially from the main memory to the processor core and caches (even for the memory-bound workloads). Second, the processor core becomes the primary source of energy consumption due to the more energy-efficient M3D main memory (see §2).

Our goal in this work is to design the core and cache hierarchy given the shifted bottlenecks in M3D systems. To this end, we take two steps. First, we explore the implications of shifted bottlenecks on the processor core and cache hierarchy design. Second, based on these implications and by leveraging the new opportunities of M3D integration, we design a new M3D-based system.

Implications of M3D Integration on Cache Hierarchy Design. Through a detailed analysis of the *depth*, *size*, and *latency* of the cache hierarchy in an M3D-based system, we make three new observations. First, all evaluated workloads

perform better or equally well in an M3D-based system with a shallow one-level cache hierarchy (i.e., with L1 caches) compared to an M3D-based system with a deeper and larger cache hierarchy (§5.1.1). Second, although M3D integration enables reducing cache latency, the benefit of removing the deeper cache levels is still higher than or comparable to increasing the sizes (§5.1.2) and/or improving the latencies of the deeper cache levels (§5.1.3). Third, in contrast to the deeper levels of the cache hierarchy, L1 caches in an M3D-based system are still critical for performance, and improving their latency improves performance for a wide range of workloads (§5.1.3).

Implications of M3D Integration on Processor Core Design. We perform a detailed analysis of different units in all stages of an out-of-order superscalar processor core pipeline. We highlight three new observations, demonstrating the most important factors impacting performance. First, larger pipeline widths improve M3D performance since they increase the number of in-flight requests, which can be effectively served given M3D’s high memory bandwidth (§5.2.1). Second, the performance impact of pipeline frontend (e.g., fetch, decode, and branch prediction units) increases significantly (§5.2.3), as M3D shifts the bottleneck away from memory, increasing the fraction of execution time dominated by these units. Third, while high-bandwidth main memory enables running many threads concurrently, the overhead of synchronization between threads in multi-threaded workloads limits performance (§5.2.4).

Re-Architecting M3D. Considering the implications of M3D integration on cache hierarchy and processor core design, we propose an optimized M3D-based system, *RevaMp3D*, based on five key design decisions. First, we remove the shared last-level cache (L2 in our M3D baseline) from the cache hierarchy. Second, we reduce L1 cache latency by devising a 3D layout for the SRAM array, in which the array is divided across two logic layers to reduce its overall wire lengths and latency. Third, we leverage the area reclaimed from removing the large cache to widen and scale up various structures in the processor pipeline that enable greater instruction-level parallelism (e.g., reorder buffer and execution units). This design accommodates more in-flight requests, which can be efficiently served due to the high M3D memory bandwidth. We avoid latency penalties from these larger structures by leveraging M3D layouts to keep their wire lengths short. Both the second and third design decision take advantage of the dense ILVs that enable efficient vertical layout of the processor structures [14, 50, 51, 53–56]. Fourth, we introduce a new fine-grained register file-level synchronization technique, which eliminates the additional latency in the memory hierarchy for synchronization. This technique is realized by using the thin ILVs to efficiently increase the register file bandwidth to support both the regular operand accesses and the synchronization-related accesses. Fifth, we leverage the M3D main memory to mitigate the performance and energy bottlenecks of the processor core. To this end, we propose a processor frontend design that memoizes the repetitive (i.e., in a loop) fetched, decoded, and reordered instructions, stores them in main memory at low cost, and turns off the relevant parts of the processor core when possible. The high-bandwidth, energy-efficient M3D main memory enables storing and loading the memorized instructions efficiently, thus eliminating the area overhead of prior memoization techniques that require a large SRAM capacity [64, 65]. This design alleviates (i) energy bottlenecks when repeated instructions execute, and (ii) branch misprediction overhead since a large fraction of instructions do not need to be fetched, decoded, and re-ordered on branch misprediction.

Key Results. We evaluate *RevaMp3D* using a heavily modified cycle-accurate architectural simulator (ZSim [66]) to flexibly explore various designs and faithfully model the M3D-based systems. We experimentally calibrate the parameters for the M3D baseline based on the fabricated device models, circuit analysis, interconnect model, and physical design tools presented in [9]. We evaluate *RevaMp3D* using a wide range of 20 real-world workloads and 7 multi-programmed mixes. On systems with 1, 16, 64, and 128 cores, *RevaMp3D* provides 1.2×–2.9× speedup and 1.2×–1.4× energy reduction across all evaluated workloads and core counts, with a 12.3% reduction in logic area, compared to the state-of-the-art M3D-based system [1, 9], while providing 4.96× and 7.14× average speedup compared

to the state-of-the-art 3D and 2D systems, respectively. As part of our design space exploration, we analyze the impact of RevaMp3D’s design decisions for M3D-based systems with various main memory latency values since memory latency can vary depending on the design decisions made to meet certain requirements of the target system. This analysis facilitates making the appropriate design decisions based on the M3D main memory latency. Our analysis demonstrates that by re-architecting M3D systems based on their shifted bottlenecks and unique opportunities provided by M3D integration, we can re-allocate the logic area to different units in the processor core and cache hierarchy more efficiently, thereby benefiting a wide range of workloads.

This work makes the following **key contributions**:

- We conduct a rigorous design space exploration of key components of the processor core and cache hierarchy to understand the implications of the M3D integration of logic and memory layers on the applications’ performance and energy bottlenecks.
- We introduce RevaMp3D, an optimized M3D-based system, based on our insights from our analysis and leveraging M3D integration’s opportunities, such as tightly-integrated logic layers and fast and energy-efficient main memory.
- We show that RevaMp3D provides significant performance improvement and energy reduction compared to the state-of-the-art M3D-based system, while achieving a smaller logic area.

2 M3D Technology

We provide a brief overview of the M3D integration technology, state-of-the-art M3D-based systems, and their technology feasibility and constraints.

M3D Integration Technology. There has been significant effort into enabling tighter integration of logic and memory layers in the system to improve performance and energy. While prefetching can be effective for many workloads, it cannot fundamentally eliminate the data movement bottlenecks inherent in modern memory systems. In particular, prefetching relies on the presence of sufficient spatial or temporal locality and becomes significantly less effective for workloads with low locality, irregular access patterns, and limited predictability [67, 68]. This is ultimately one of the key reasons for the substantial efforts in industry and academia (e.g., [1–27, 29–33]) on developing 3D and M3D integration technologies to connect the device layers more tightly. Such architectures aim to fundamentally reduce data movement overhead, rather than relying solely on speculative techniques to tolerate latency.¹

Fig. 1 compares three different systems. In 2D systems, computation and memory units are connected via off-chip links with low bandwidth, which is imposed by the limited number of I/O pins in the memory system. In 3D systems [15–20, 69–76], memory layers are connected using Through-Silicon Vias (TSVs) or hybrid bonding and can be connected to logic units directly below the memory layers using TSVs/hybrid bonding or on an interposer substrate. Compared to 2D systems, 3D systems provide higher main memory bandwidth, lower latency, and better energy efficiency. In M3D-based systems [1–3, 5–10], logic and memory layers are *monolithically-fabricated on the same chip* with a large number of thin Inter-Layer Vias (ILVs) with very small pitch sizes (e.g., <100 nm [1, 9, 14]). Compared to TSV, which has a pitch size of ~2.6–25 μm [14, 77], and hybrid bonding, which has a pitch size of ~0.3–10 μm [15–20], the smaller pitch size of ILVs enables a much denser inter-layer connectivity.

There are two classes of M3D-based systems: (i) *only* with logic layers and (ii) with *both* logic and memory layers. The first type provides several optimization opportunities, such as efficient 3D partitioning of logic structures (e.g., caches, NoCs) to reduce their latency by shortening the wires [14, 50]. The second type enables additional benefits by

¹Note that techniques such as prefetching or other microarchitectural techniques can also orthogonally be used in 3D/M3D architectures when needed.

significantly alleviating the main memory bottlenecks [1, 9, 78, 79]. In this work, we consider the second type. High memory bandwidth is realized by the dense ILVs between logic and memory layers. Low memory latency is achieved due to three reasons. First, the high-bandwidth ILVs enable efficiently devising a large number of memory channels, each connected to relatively small memory arrays. The smaller wire lengths in these arrays lower overall access latency, and the larger channel counts lower the contention across concurrent memory accesses. Second, the low pitch size of the ILVs enables efficient M3D layouts of memory arrays (e.g., placing different banks in a memory channel in different layers). This allows further reduction of wire lengths in a memory array and, subsequently, reduction in the array’s latency.² Third, short and dense ILVs lead to low-latency interconnection between logic and memory on the same chip.

Baseline Architecture. We use N3XT [1, 5, 7–9], a state-of-the-art M3D-based system, as our baseline. N3XT leverages emerging technologies such as carbon-nanotube-based transistors in the logic layer [2, 5, 7] and latency-optimized monolithic 3D RRAM arrays in the memory layers [80, 81]. The fabrication and thermal feasibility of the N3XT architecture has been demonstrated by real prototypes [7]. Fig. 2 shows the baseline M3D architecture [9], integrating several logic layers (one for processor cores, one for cache access circuitry, one for shared L2 cache, two for interconnection network to enable high-bandwidth communication between main memory and cores, one for memory access circuitry and memory controllers) and memory layers (64 RRAM layers). Note that the 3D layout of interconnection networks leads to reduced wire lengths and a reduced overall planar footprint [82–84]. This is achieved by utilizing vertical connections to traverse layers, which are significantly shorter than the planar distances required in 2D layouts.

In this work, although we use N3XT as our baseline M3D-based system, we primarily focus on characteristics such as main memory bandwidth and latency rather than device-specific features. Because we evaluate M3D-based systems using a range of parameters (e.g., main memory latency), our insights can be broadly applied to enhance performance and energy efficiency in M3D-based systems that employ different logic and memory device technologies.

Technological Feasibility and Constraints. Prior work shows that both logic and memory layers in N3XT can be fabricated at *low temperatures* ($<300^{\circ}\text{C}$ [1, 9]). This paves the way to fabricating layers monolithically on top of each other in the same chip without the top layers melting the lower layers during fabrication. Some recent works even demonstrate the feasibility of M3D fabrication using commercial silicon facilities [1, 85]. Such works facilitate the wider adoption of M3D integration technology by alleviating the need to devise completely new fabrication lines for M3D. Despite all the benefits, there are two key challenges and constraints for M3D fabrication. First, since the M3D fabrication process is sequential (i.e., device layers need to be monolithically and sequentially integrated on top of each other, as opposed to 3D-stacked devices where layers can be fabricated in parallel), M3D technology suffers from concerns typically regarding increased cost and reduced yield. Second, RRAM, the memory technology used in the baseline M3D-based system considered in this work, has limited write endurance. N3XT addresses this issue using online data relocation wear-leveling, extending the device lifetime to at least 10 years [9]. We incorporate the same

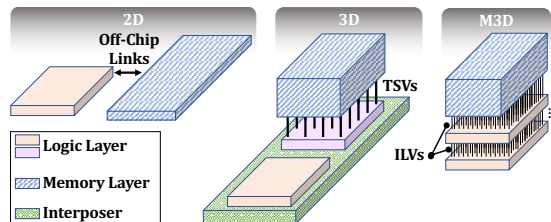


Fig. 1. Systems with 2D, 3D, and M3D integration.

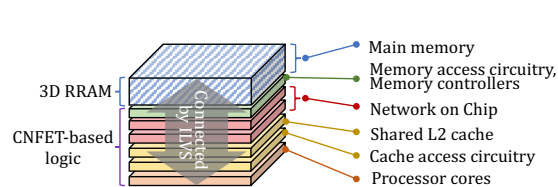


Fig. 2. Overview of the baseline M3D-based system [9].

²Note that larger pitch sizes of other 3D integration technologies reduce the benefits of fine-grained 3D partitioning of memory arrays [14].

solution in our evaluations (§3). We consider the investigation of more efficient solutions (e.g., [86, 87]) for addressing device challenges as a critical and orthogonal direction.

3 Methodology

3.1 Workloads

Table 1 summarizes the wide range of multi-threaded workloads used in our analysis, selected from DAMOV [67], which is a benchmark suite for main memory data movement studies. DAMOV aggregates workloads from diverse benchmark suites, including workloads that (1) represent different types of data movement bottlenecks, and (2) come from a wide range of application domains. This is particularly well-suited for our analysis because our goal in this work is to architect the system with monolithically integrated logic and memory layers, where main memory bottlenecks are significantly alleviated. Table 1 also lists the inputs or settings used for each workload. All the workloads and the input files can also be downloaded from the DAMOV benchmark suite repository [67, 94].

To gain an understanding of our workload’s data movement bottlenecks, we perform a *top-down analysis* [95], a widely-adopted approach that hierarchically characterizes the workload bottlenecks [95–98]. We use the Intel VTune Profiler [99] to perform the top-down analysis. For each workload, Table 1 shows the backend-bound (BE), DRAM-bound (Mem), and DRAM bandwidth-bound (BW) values obtained from VTune, while running on Intel Xeon E3-1240 processor with 4 cores. BE accounts for the percentage of execution time during which the processor cannot issue new instructions due to stalls at the pipeline backend, including stalls due to memory requests and core execution (e.g., no empty free slot in the execution unit of the pipeline). The stall due to memory requests further divides into stalls due to caches or DRAM (Mem). Mem can be further split into DRAM latency- and bandwidth-bound (BW). Table 1 also shows Last-to-First Miss Ratio (LFMR), a metric proposed for showing the effectiveness of caches [67], which is obtained by dividing the number of L2 cache misses (last-level cache in our M3D baseline) by the number of L1 cache misses. A high LFMR suggests that the L2 cache does not provide significant benefits in reducing the miss rate. We consider LFMR above 90% as high, as most requests are not serviced by the L2 cache.

Table 1. List of workloads and their input sizes.

Class	Workload	Suite	Domain	Input	Size (MB)	BE(%)	Mem (%)	BW (%)	ILP	LFMR
Bandwidth-bound	YOLO	Darknet [88]	Machine Learning	ref	204	94.17	62.01	56.60	2.25	0.99
	BFS	Ligra [89]	Graph Processing	rMat	2017	44.94	59.14	40.56	1.71	0.98
	BC	Ligra [89]	Graph Processing	rMat	2017	75.72	65.16	56.84	2.09	0.99
	KCore	Ligra [89]	Graph Processing	rMat	2017	94.54	44.88	78.68	1.62	0.99
	MIS	Ligra [89]	Graph Processing	rMat	2017	86.70	71.72	90.88	2.02	0.99
	PageRank	Ligra [89]	Graph Processing	rMat	2017	86.70	71.72	90.88	2.02	0.99
Latency-bound	Radii	Ligra [89]	Graph Processing	rMat	2017	54.12	43.10	66.34	1.78	0.99
	StreamCluster	Rodinia [90]	Data Mining	ref	67	63.84	43.22	17.38	1.74	0.99
	ResNet	Darknet [88]	Machine Learning	ref	230	62.66	55.00	26.74	2.25	0.99
	Oceanncp	Splash-2 [91]	HPC	simlarge	17	92.98	47.02	22.12	6.63	1
	Components	Ligra [89]	Graph Processing	rMat	2017	50.94	42.12	6.62	1.38	0.99
	Triangle	Ligra [89]	Graph Processing	rMat	2017	62.08	51.10	18.74	1.41	0.99
Compute-bound	Myocyte	Rodinia [90]	Simulation	1000000	364	93.44	89.26	29.92	1.88	0.99
	3mm	PolyBench [92]	Linear Algebra	simlarge	128	60.3	13.8	34.68	2.75	0.61
	2mm	PolyBench [92]	Linear Algebra	simlarge	128	62.50	13.8	35.29	2.55	0.60
	atax	PolyBench [92]	Linear Algebra	simlarge	512	25.50	1.60	14.9	2.37	0.51
	gemm	PolyBench [92]	Linear Algebra	simlarge	96	63.4	13.8	23.11	2.55	0.58
	ferret	PARSEC [93]	Similarity Search	ref	47	29.22	4.5	0.5	2.64	0.61
	Needleman-Wunsch	Rodinia [90]	Bioinformatics	ref	4295	79.96	39.66	65.46	2.35	0.52

Based on this characterization, we classify the workloads into *main memory bandwidth-bound*, *main memory latency-bound*, and *compute-bound*. We categorize the workloads with large BE (>40%), Mem (>40%), and BW (>50%) as DRAM bandwidth-bound since we observe large performance improvements when improving the main memory bandwidth for these workloads. We categorize workloads with high BE and Mem and low BW as DRAM latency-bound since we observe large performance improvements when improving the main memory latency for these workloads. We categorize workloads with high BE and low Mem as compute-bound. When a workload nearly misses the border between main memory-/compute-bound, we use LFMER to classify the workload as memory-bound (LFMER>90%) or compute-bound.

For our end-to-end evaluations, we also evaluate a wide range of multi-programmed workload mixes, with a focus on combining workloads with various bottlenecks. We summarize the multiprogram workload mixes in Table 2.

Table 2. Workloads used in our analysis.

Class	Mix	Workloads
	1	Components + 3mm
Memory-bound +	3	MIS + atax
Compute-bound	6	PageRank + 2mm
	7	Triangle + gemm
Memory-bound + Memory-bound	5	Oceanncp + StreamCluster
Compute-bound +	2	gemm + atax
Compute-bound	4	NW + 3mm

3.2 Experimental Setup

Modeled Systems. We use a cycle-accurate architectural simulator (ZSim [66]) to flexibly explore various designs and faithfully model the following systems:

- **2D:** a system based on the 2D integration of computation and memory, where the cores and main memory (DRAM) communicate through an off-chip bus.
- **3D:** a system that uses TSVs to integrate memory layers, which connect to compute units via interposers (e.g., [13]). We consider six HBM stacks connected to compute units similar to a state-of-the-art 3D system [105].
- **M3D:** a system based on N3XT [1, 5, 7–9], where memory and logic are monolithically fabricated on each other. We experimentally calibrate the M3D-based system parameters based on the fabricated device models, circuit analysis, interconnect model, and physical design tools presented in [9]. The latency of on-chip main memory in the M3D-based system can depend on various factors (e.g., memory capacity, size of each memory array, and length of local and global wires in the memory array). Therefore, to gain comprehensive insights into M3D-based system design implications, we also evaluate M3D-based systems with varying memory latency values in our design space exploration (§5) and

Table 3. 2D, 3D, and M3D system configurations.

System	M3D	3D	2D
Main Memory	64 GB on-chip 3D RRAM [9]; Up to 16 TB/s [9]; FR-FCFS scheduling; 5/13ns R/W (up to 5/60ns R/W); 0.8/1.1 pJ/bit R/W [9]	64 GB on-chip 3D-stacked DRAM using 5um TSVs; HBM2 interface, 1.5 TB/s [12, 13]; FR-FCFS scheduling; 51/55ns R/W; 9 pJ/bit [9]	64 GB off-chip DRAM; DDR4 interface, 102 GB/s [100]; FR-FCFS scheduling; 65/60ns R/W [9]; 20pJ/bit R/W [101]
L3	None	None	Shared 8 MB, 16-way, 27-cycle; 945/1904 pJ per hit/miss [102]
L2	Shared 256 KB per core (0/1/8/64 MB) 8-way, 12-cycle (6-cycle); 46/93 pJ per hit/miss	Shared 256 KB per core, 8-way, 12-cycle; 46/93 pJ per hit/miss	Private 256 KB per core, 8-way, 12-cycle; 46/93 pJ per hit/miss
L1	32 KB, 8-way, 4-cycle (2-cycle); 15/33 pJ per hit/miss [102]		
Processor Core	1/16/64/128 out-of-order cores @ 4 GHz; 4-wide pipeline (8-wide); 128-entry reorder buffer (256-entry); Branch predictor: two-level GAs [103] (TAGE-SC-L [104] and ideal predictor with no mispredictions); 0.48 nJ/inst for M3D; 1.5 nJ/inst for 2D and 3D		

end-to-end evaluations (§7). To this end, we rigorously sweep the memory latency values from half the value reported for the baseline M3D configuration up to a latency value similar to the baseline 2D system.

We summarize all system parameters in Table 3.³ We also show other configurations analyzed in §5 in parentheses. **Cache and Core.** We initially consider the same core and L1 caches for all configurations. 2D has a deeper and larger cache hierarchy compared to 3D and M3D since it has the lowest available memory bandwidth. We consider a cache hierarchy for M3D similar to N3XT [9] (private L1 and shared L2). We consider the same cache hierarchy for 3D. In §5, we study the effects of different cache and core configurations in M3D.

Main Memory. In our analysis, all three systems have large enough main memory capacity to contain the working set of all applications in Table 1.⁴ Although the main memory in the M3D baseline is RRAM-based and different from DRAM used in 2D and 3D, in our performance analysis, we primarily distinguish memory systems by their bandwidth and latency and not their other device features. As explained in §2, in our evaluations, we employ the same technique used in the M3D baseline for alleviating the reliability and endurance issues of the RRAM-based memory [9].

Network on Chip. The M3D baseline [9] uses the meshes of trees (MoT) [106] scheme to provide a high-bandwidth connection between the cores and the memory controllers. This network supports uniform memory access (UMA) such that each core has the same access latency to any memory channel.

4 Motivational Analysis

We conduct an experimental analysis of performance and energy bottlenecks of a variety of workloads on a state-of-the-art M3D-based system.

4.1 Performance Bottlenecks

We evaluate the performance benefits of the M3D-based system over the 2D and 3D systems across *all our evaluated workloads*. Fig. 3 shows the performance⁵ of 2D, 3D, and M3D baselines with different core counts, averaged across all our workloads. Our analysis shows that the M3D system provides significant benefits over 2D and 3D baselines, delivering 2.8× and 4.0× average speedups over 2D and 3D systems, respectively.

To show how the M3D affects the performance bottlenecks of the conventionally main memory-bound workloads, we compare the performance bottlenecks of *memory latency-/bandwidth-bound* workloads. To this end, we extend ZSim [66] by incorporating the top-down bottleneck analysis [95]. We validate our implementation of the top-down analysis in ZSim by comparing its output against Intel VTune Profiler [99] running on Intel Xeon E3-1240. Our validation shows that the ZSim-based top-down analysis identifies very similar *trends* in bottlenecks as Intel VTune [99], showing a high Pearson correlation value [107] of 93.94% ($P < 0.001$) across our workloads. Fig. 4 and Fig. 5 show top-down bottleneck breakdown of representative latency-bound (Tri) and a bandwidth-bound (BFS) workloads. In the M3D-based system,

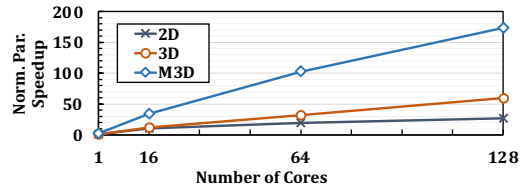


Fig. 3. Performance benefits of the M3D-based system over the 3D and 2D systems.

³The main memory latency values in this table refer to average main memory access latency.

⁴We also discuss the case where data does not fit in one stack in § 8.

⁵Performance refers to the normalized parallel speedup, where all values are normalized against that of the 2D baseline.

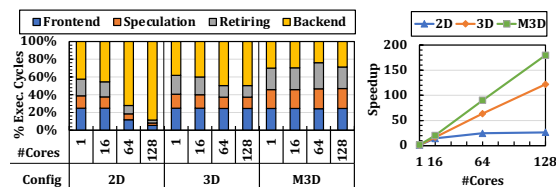


Fig. 4. Bottlenecks of a latency-bound workload.

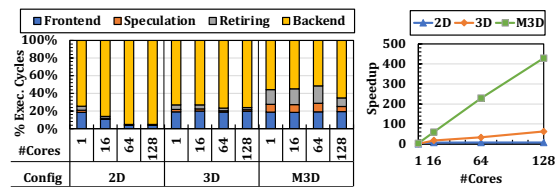


Fig. 5. Bottlenecks of a bandwidth-bound workload.

we observe a large reduction in the ratio of execution time spent on the backend, compared to 2D and 3D, and a substantial *bottleneck shift* in the system from the backend to the frontend and speculation.

To gain a deeper understanding of the backend bottlenecks (which are influenced by the main memory, cache hierarchy, and the processor’s functional units), we study an *idealized* M3D-based system with a one-cycle main memory latency and no main memory bandwidth bottleneck.⁶ We observe that even such a configuration only leads to a 23% speedup, lowering the backend bottleneck only by 5%, which means that the main memory is not a key contributor to the M3D-based system’s backend bottleneck. We conclude that the advancements in M3D memory performance result in substantially *shifting* the application bottlenecks from main memory to other parts of the system.

Takeaway 1. *The advancements in M3D memory performance substantially shift the applications’ performance bottlenecks from main memory to other parts of the system.*

4.2 Energy Bottlenecks

We analyze the energy bottlenecks in different system and observe that, compared to the 2D (3D) systems, the M3D-based system consumes on average $4.32\times$ ($4.76\times$) and $4.13\times$ ($3.32\times$) lower energy on compute-bound and memory-bound workloads, respectively. Even though for the memory-bound workloads, the main memory consumes a significant percentage of the overall energy in 2D and 3D, the main memory in the M3D baseline contributes to only 12% of total energy, turning the processor core into the most prominent contributor to the total energy consumption in M3D.

The energy benefits of the M3D baseline are due to two key factors. The first factor is related to the device-level advances in logic and memory layers, which, in fact, are orthogonal to the M3D integration. For example, the CNFET-based memory access circuits consume less power compared to MOSFETs [2], and the deployed RRAM-based memory layers are more energy-efficient than DRAM [7–9]. The second factor is related to the M3D integration. As discussed in §2, M3D integration efficiently supports many memory channels, each connected to smaller memory arrays. Due to the shorter wire lengths within the memory arrays and the shorter global wires connecting the memory layers to logic layers on the same chip, the overall energy of memory accesses gets lowered with M3D integration.

Takeaway 2. *In the M3D baseline, the processor core turns into the most critical energy bottleneck.*

4.3 Our Goal

Given the opportunities provided by M3D to drastically shift the performance and energy bottlenecks, it is important to understand the implications of this new technology on processor core and cache hierarchy designs that have been conventionally specialized to tackle main memory bottlenecks. **Our goal** in this work is to design the core and caches, given the new trade-offs of M3D. While we focus on architecting M3Dsystems in this work, we argue that if other

⁶We do not change load/store queues or caches in this case.

integration technologies (e.g., TSV or hybrid bonding) in the future achieve the same properties (e.g., pitch sizes) as current M3D technologies, our architectural insights can also be applied to systems with such integration technologies.

5 Architecting the Processor Components

To design general-purpose processors based on the new opportunities and shifted bottlenecks of M3D-based systems, we analyze the design trade-offs of the cache hierarchy (§5.1) and cores (§5.2) in M3D. Table 4 summarizes (i) the key structures analyzed in this work, in different stages of an out-of-order superscalar processor core pipeline, (ii) the key analyzed aspect of each structure, and (iii) a pointer to the relevant sections.

Table 4. Analyzed pipeline elements.

Stage	Key Structure	Analyzed Aspect	Ptr.
Fetch	Instruction cache Branch predictor	Part of frontend bottleneck	§5.2.3
		Speculation bottleneck	§5.2.3
		Part of pipeline width	§5.2.1
Decode	Pre-decoder Decoder	Part of frontend bottleneck	§5.2.3
		Part of pipeline width	§5.2.1
Issue	Instruction window Reorder buffer	Part of pipeline width	§5.2.1
		Reorder buffer size	§5.2.2
Execution	Functional units	Part of pipeline width	§5.2.1
		Latency of micro-operations	§5.2.5
Memory	L1/L2 data caches Load/store queues Threads communication	Cache size, latency, depth	§5.1
		Load/store queue sizes	§5.2.2
		Synchronization	§5.2.4
Writeback	Register file (RF)	Part of pipeline width	§5.2.1

5.1 Cache Hierarchy

The design space of the cache hierarchy in M3D-based systems is affected by two conflicting factors. On one hand, M3D integration enables reducing the latency of caches through efficient 3D layouts (e.g., [53–56]) that reduce wire lengths. On the other hand, as discussed in §2, M3D integration enables improving main memory performance (bandwidth and latency), which reduces the impact of caches on the application performance. We evaluate the impact of these conflicting factors on the performance of a wide range of workloads running on the M3D-based system.

5.1.1 Depth of the Cache Hierarchy. We compare noL2, an M3D-based system with no L2 cache⁷, and w/L2, an M3D-based system with a shared L2 cache. Fig. 6 shows the performance of noL2 normalized to w/L2 across all our workloads on an M3D system with 64 cores, showing on average 11.5% speedup of noL2 over w/L2.

To provide a more detailed analysis of the impact of removing the L2 cache, Fig. 7 shows the performance of a representative workload with low LFMR (atx) alongside the Average Memory Access Time (AMAT) and cache miss rates for a 64-core system. We observe that, despite having a low L2 cache miss rate of 19% in w/L2 and a faster L2 compared to the M3D main memory, removing the L2 cache does not hurt performance.⁸ Second, we observe that the

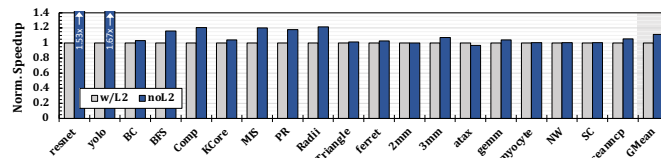


Fig. 6. Performance of the M3D-based systems with and without the L2 cache.

⁷Coherency is still maintained using a shared directory.

⁸Prior work (e.g., [108, 109]) has shown that removing shared caches can be effective for workloads with high cache miss rates, but it can degrade performance for workloads with strong cache locality [109]. In contrast, our results demonstrate that the improved memory performance in M3D enables removing shared caches without negatively affecting either class of workloads.

AMAT in noL2 is on par (even 4% lower) with the AMAT in w/L2. While removing L2 does not significantly hurt AMAT for workloads with high L2 hit rates in M3D, removing it in the 3D baseline can lead to an up to 17× larger AMAT due to its slower main memory. Fig. 8 shows the performance, AMAT, and cache miss rates of a representative workload with high LFMER (MIS) for the same configurations. Based on this figure, we make three observations. First, noL2 improves performance by 17.8% on average across all core counts compared to both configurations with L2. Second, the L2 cache is highly ineffective (99% misses) in filtering accesses to the main memory. Third, the AMAT in noL2 is significantly lower than the two other configurations since it does not add extra L2 access latency and contention overhead.

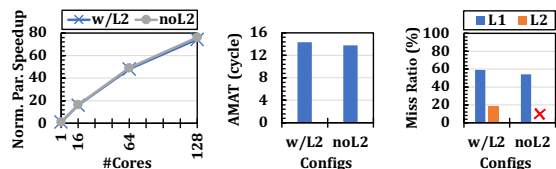


Fig. 7. Effect of no L2 cache on a low LFMER workload.

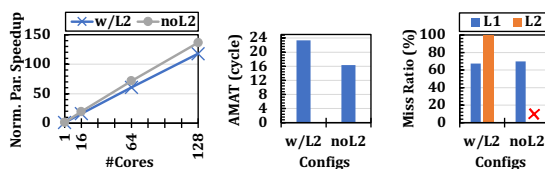


Fig. 8. Effect of no L2 cache on a high LFMER workload.

Takeaway 3. *In the M3D baseline, removing the shared L2 cache does not degrade performance, and even leads to improved performance for some workloads.*

Due to the importance of analyzing the impact of M3D architectural design decisions on an M3D system with different latency values (as discussed in §3), we demonstrate the impact of cache hierarchy for an M3D system with different memory latency values. We keep the memory bandwidth the same (as listed in Table 3) across configurations. Fig. 9 shows the performance of a low-LFMER workload on an M3D-based system with 64 processor cores in two different cases: (i) a configuration with no L2 (noL2), and (ii) a configuration with no L2, and where the area originally dedicated to L2 is used to increase the processor core’s pipeline width (Wide+noL2), as explained in §5.2.1 and §6. For each latency value, performance is normalized to the M3D baseline (with L2 cache and baseline pipeline width) with that latency. We observe that even until 4× larger latency values, it is beneficial to use the logic area for increasing processing capability (e.g., wider pipeline) instead of larger caches. This is because the large M3D bandwidth enables serving a larger number of in-flight requests. However, for larger latency, having larger caches becomes critical. In §7, we analyze the impact of all of RevaMp3D’s design decisions in M3D-based systems with different latency values across all our workloads.

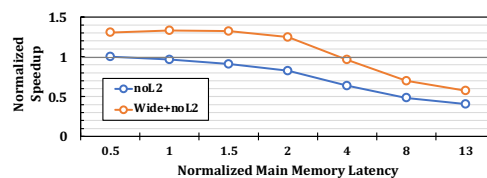


Fig. 9. Performance impact of removing the L2 cache on M3D-based systems with different memory latency values.

Takeaway 4. *Even until 4× larger main memory latency values (compared to the M3D baseline), it is beneficial to use the logic area for increasing processing capability (e.g., a wider pipeline) instead of increasing the cache sizes. This is because the M3D main memory enables efficient serving of a large number of in-flight requests. However, for higher latency values, having larger caches becomes critical.*

Microarchitectural implications. We detail the architectural implications of removing the L2 cache in the M3D system by explaining four key aspects. First, removing the shared L2 cache increases main memory accesses for some workloads, but the wear-leveling provisions in the M3D baseline remain sufficient for maintaining lifetime guarantees even in this case. This is because the M3D baseline is already designed to meet its reported lifetime guarantees under the worst-case scenarios: workloads where caches are ineffective at filtering main memory accesses. This is common in memory-bound workloads, as also observed in our evaluations (characterized by high LFM values in Table 1). While compute-bound workloads incur more memory accesses when the L2 cache is removed, their *total access count* remains well below that of memory-bound workloads. To confirm this, we analyzed the maximum number of writes per cycle across all workloads, with and without the L2 cache. We found that the maximum writes/cycle (2.42 for the 64-core configuration) is *unchanged* in both cases. This is because the worst-case write rate originates from the highly memory-bound workload BC, which has low access locality and an L2 miss rate of 99%. In contrast, compute-bound workloads, which benefit from higher data locality, show significantly lower writes/cycle even without L2 (up to 8x lower than BC). Since removing L2 does not worsen the worst-case write behavior, the baseline wear-leveling technique [9] remains sufficient to achieve the same endurance as the M3D baseline [1, 5, 7–9].

Second, removing the L2 cache in the M3D baseline does not introduce notable energy penalties, and in fact, our overall design (as evaluated in §7) improves energy efficiency. For compute-bound workloads, removing the L2 cache increases the number of memory accesses and the activity of the memory controller. However, in these workloads, given M3D’s energy-efficient main memory, most of the energy consumption is due to the processing units (as shown in §4.2). Furthermore, the M3D baseline’s memory controller consumes very little energy (~ 0.01 pJ/bit per controller) [9], which is negligible, even compared to M3D’s main memory. For memory-bound workloads, removing L2 caches leads to only an intangible impact since the L2 cache is highly ineffective at filtering the memory accesses. Overall, as demonstrated by the RvM3D-P configuration in Fig. 26 (considering only our proposed performance optimizations), removing the L2 caches leads to only a modest 2% increase in average energy consumption. Finally, when considering both our proposed performance and energy optimizations, the overall design (RvM3D in Fig. 26) results in even lower (by $1.2\times$ – $1.4\times$) energy consumption than the M3D baseline.

Third, removing the L2 cache naturally disables L2 prefetching; however, this has minimal impact on performance. This is because, as observed in this section, even for workloads with high L2 hit rates, the absence of the L2 cache leads to comparable performance due to M3D’s highly efficient main memory. L1 prefetching remains possible in this configuration, which can be used for workloads that benefit from it.

Fourth, removing the L2 cache does not impact the process of context switching itself, as the contents of the caches are not checkpointed during context switches. While the presence of the L2 cache may preserve some program data in the cache across context switches, as shown in this section, even for workloads with high cache hit rates, the L2 cache provides minimal performance benefit (and on average, across all workloads, removing L2 leads to speedups). We demonstrate the impact of removing the L2 cache on context-switching by comparing 16-core M3D systems with and without the L2 cache. Fig. 10 shows the performance of the multi-program workload mixes in Table 2, with each

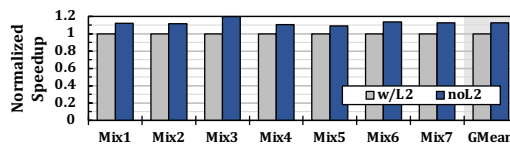


Fig. 10. Effect of removing the L2 cache on context switches.

workload in the mix using 16 threads. We observe that the configuration without L2 performs on average 12.7% better than the configuration with L2.

5.1.2 Impact of Cache Size. We analyze the performance implication of increasing the L2 cache size. M3D facilitates circuit-level and device-level optimizations to increase cache size or reduce cache latency by designing vertical layouts of SRAM arrays to reduce the overall wire lengths. Analyzing the effects of such optimizations on M3D-based systems with logic and memory layers enables us to decide whether removing L2 in such systems is ultimately better than optimizing it. We analyze the performance of workloads with low and high LFRM, with varying L2 sizes and no L2. Even though increasing cache size can increase latency, we optimistically consider the ideal case where the latency does not increase with the cache size. Across *all evaluated workloads* with different core counts, increasing the cache size leads to only a 3.7% average speedup.

Takeaway 5. *In the M3D baseline, increasing the L2 cache size does not significantly outperform removing it.*

5.1.3 Impact of Cache Latency. We study the effect of reducing the latency of L1 and L2 caches. We analyze M3D-based system configurations where (i) the L1 latency is improved by $2\times$ (L1fast), and (ii) the L2 latency is improved by $2\times$, and the L2 size is 64MB (L20pt). Overall, we observe 12.5%/6% average speedup due to L1/L2 latency reduction across *all evaluated workloads*. We conclude that removing the shared L2 cache leads to better or comparable performance compared to larger or faster L2 caches. However, it is still important to reduce L1 latency. This is because L1 cache latency represents a large portion of the AMAT in M3D due to M3D’s fast main memory.

Takeaway 6. *In the M3D baseline, removing the shared L2 cache leads to better or comparable performance compared to faster L2 caches. However, it is still important to reduce the latency of the L1 cache.*

5.2 Processor Core Design

5.2.1 Impact of Pipeline Width. We aim to understand the impact of wider pipelines in the M3D-based system. Wider pipelines lead to a higher number of in-flight requests, which can be beneficial when the main memory can serve requests efficiently. Fig. 11 shows the performance of a 64-core M3D system with doubled pipeline width normalized to the performance of a 64-core baseline M3D system. Across all our workloads, we observe a 32.3% average speedup.

To differentiate the impact of pipeline width on the performance of 2D, 3D, and M3D-based systems, in Fig. 12, we show an example of a bandwidth-bound workload (BFS) on these systems when doubling the pipeline width. Each data point is the speedup of each configuration after widening the pipeline over *the same configuration*. We observe that doubling the pipeline width provides a 40% speedup in the M3D-based system, while providing a lower speedup in the 2D and 3D systems. This is because, with large core counts, main memory bandwidth becomes a major performance bottleneck in the 2D and 3D systems and cannot service a higher number of requests from the wide pipeline.

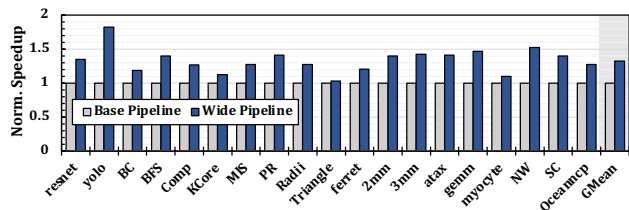


Fig. 11. Speedup of an M3D system with a wider pipeline.

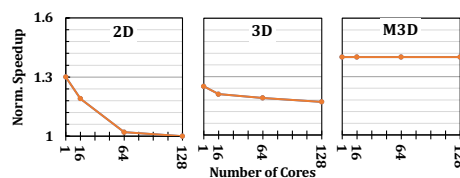


Fig. 12. Speedup of the wide pipeline for 2D, 3D, M3D.

We also analyze the effects of increasing the widths of different pipeline stages separately to understand whether significant benefits are obtained at lower area costs. We observe that doubling the width of *both* the backend and frontend leads to at least $1.27\times$ higher average speedup (across all our evaluated workloads) than doubling the widths individually. As discussed in §5.1.1, Fig. 9 shows the performance of a wider pipeline on M3D-based systems with high memory bandwidth but varying memory latency values.

Takeaway 7. *Wider pipelines provide large benefits to the M3D baseline.*

5.2.2 Size of Reordering Structures and Queues. We analyze the performance of the wide pipeline with (i) baseline load/store queues (L/SQ), issue queue, and reorder buffer (ROB) depths and (ii) two times deeper queues. Across all evaluated workloads, larger queue sizes have a lower performance impact on the M3D-based system compared to the 3D system (on average, 12% in M3D versus 25% in 3D) due to lower instruction wait times in the M3D-based system. Despite the relatively lower impact of queue sizes in the M3D-based system, some workloads still take significant advantage of the larger queues (e.g., up to 20%).

We further increase the ROB size to 512 entries and continue to observe relatively low average speedup, but with particularly larger benefits for a subset of applications. Relative to a configuration with a 256-entry ROB, this results in speedups of up to 17%, with an average improvement of 3.5% across all our evaluated workloads.

Takeaway 8. *Although deeper queues provide a smaller average performance benefit in the M3D-based system than in 2D and 3D systems, a subset of workloads continue to benefit noticeably from increased queue depths.*

Increasing queue depths is not universally beneficial. In particular, increasing the issue queue’s depth increases the number of cycles spent in the issue stage, which can negatively impact the performance of *speculation-bound* workloads. Our analysis shows up to a 9.4% slowdown (for the speculation-bound workloads) due to the larger pipeline fill time and pipeline bubbles on branch mispredictions. However, as we show in §6.2, we can use the M3D-based system’s main memory to reduce this overhead for speculation-bound workloads.

5.2.3 Impact of Pipeline Frontend and Branch Prediction Units. Due to the increased impact of the frontend and speculation bottlenecks in M3D, we further study their implications on performance. For a representative speculation-bound workload (Triangle), Fig. 13 shows the performance of the baseline M3D-based system (Base) compared to M3D-based systems with (i) a state-of-the-art branch predictor [104] (TAGE-SC-L), (ii) an idealized frontend where the issue and dispatch structures in the pipeline take only one cycle (Shallow, i.e., a shallow pipeline that reduces the number of pipeline bubbles and fill latency in the event of branch misprediction), and (iii) an *idealized* branch prediction scheme, which leads to zero branch misprediction (Ideal-spec). First, we observe that while Ideal-spec leads to a $2.3\times$ speedup compared to the baseline M3D-based system, using TAGE-SC-L [104] provides only a 14% speedup.

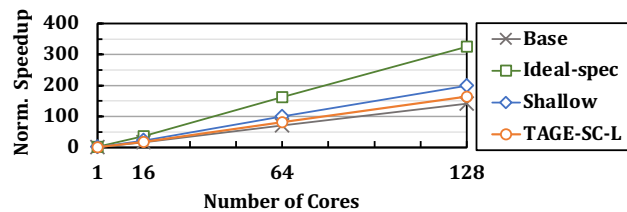


Fig. 13. Effect of speculation and frontend overheads.

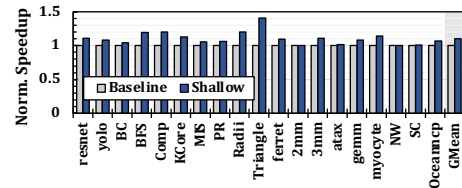


Fig. 14. Performance benefits of an M3D system with a shallow pipeline.

This is due to the large number of hard-to-predict branches in this workload. Second, by reducing the overhead of branch misprediction, *Shallow* leads to up to 41% speedup for the speculation-bound workload. Fig. 14 demonstrates the speedup of *Shallow* over the baseline 64-core M3D system across all our evaluated workloads, showing 10% average (40% maximum) speedup. §6.2 shows how RevaMp3D leverages the high-bandwidth M3D main memory to alleviate the misprediction overhead and frontend bottlenecks in the M3D-based systems with varying memory latency values.

Takeaway 9. *Improving the processor core’s frontend can lead to significant performance benefits by lowering the overhead of branch misprediction in the M3D baseline.*

5.2.4 Inter-Thread Communication. The large bandwidth of the M3D main memory can enable efficient feeding of data to a large number of threads. To take advantage of this high bandwidth, it is crucial to support efficient inter-thread communication. Fig. 15 shows the speedup of four microbenchmarks [110, 111], representing four commonly-used synchronization primitives in multi-threaded applications. We show the speedup of an M3D configuration where no overhead due to cache and memory latency is incurred during synchronization (*Opt-sync*),⁹ over an M3D configuration with baseline coherence-based synchronization (*Base-sync*). We observe on average 1.88× and up to 2.51× speedup.

We analyze the performance impact of synchronization overhead on M3D-based systems with large main memory bandwidth but with varying main memory latency values. Fig. 16 shows the speedup of an M3D configuration where no overhead due to cache and memory latency is incurred when performing synchronization over an M3D configuration with baseline coherence-based synchronization for a synchronization-heavy workload, *Radii*. We observe that the synchronization overhead increases on M3D-based systems with larger memory latency values.

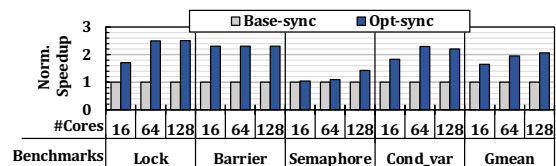


Fig. 15. Speedup of the optimized synchronization for different synchronization primitives.

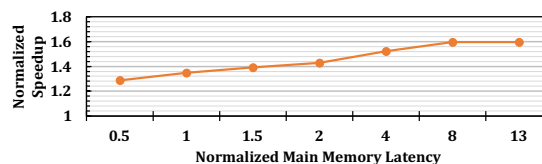


Fig. 16. Speedup of the optimized synchronization on M3D-based systems with different memory latency values.

Takeaway 10. *Reducing synchronization overhead can provide significant performance benefits for the M3D baseline.*

5.2.5 Latency of Non-Memory Micro-Operations. We model an M3D-based system where *all* μ ops take one cycle and observe only a 5.4% average speedup compared to the M3D baseline for compute-bound workloads since most functional units are pipelined. We conclude that lowering the μ ops latency does not lead to significant speedup in M3D.

While in this work, we focus on the general-purpose processor cores and caches, §8 briefly discusses the new opportunities of M3D for other parts of the system stack and for domain-specific systems.

6 RevaMp3D: Architecting Processor Core and Cache Hierarchy Based on Implications of M3D Integration

We present RevaMp3D, an optimized M3D-based system, based on the implications of M3D integration on cache hierarchy and processor core design. We target performance bottlenecks in the M3D-based system and take advantage of opportunities offered by the M3D integration technology. Fig. 17 shows an overview of the key design decisions in

⁹We consider horizontal wire delay (which also exists in the baseline) and only reduce the overhead of accessing the cache and main memory for synchronization variables.

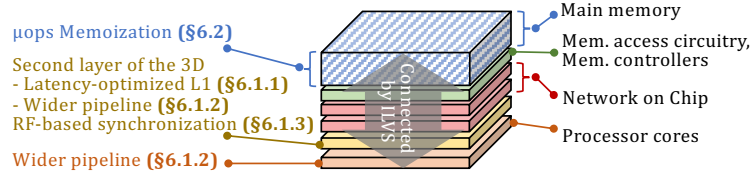


Fig. 17. Overview of the key design decisions in RevaMp3D.

RevaMp3D. §6.1 describes how RevaMp3D leverages the tight connectivity between M3D logic layers and §6.2 shows how RevaMp3D leverages M3D main memory to realize these design decisions.

6.1 Leveraging M3D Logic Layers

6.1.1 Cache Hierarchy. As described in §5.1, even an optimized L2 cache (with increased size or reduced latency) does not significantly outperform the configuration with no L2 cache. Hence, we remove the L2 cache from the cache hierarchy in RevaMp3D, which leads to freeing up 32% of the logic area. We then use this freed-up area for optimizations that alleviate the core bottlenecks and to widen and scale up various structures in the processor pipeline that enable greater instruction-level parallelism (§6.1.2). As described in §5.1, improving the L1 cache latency improves M3D performance due to the small AMAT in the M3D-based system. The short ILVs of the M3D integration technology enable efficient division of the SRAM structures between two logic layers to reduce the overall wire lengths in the SRAM structures, leading to reduced latency [14, 53–55]. Therefore, we leverage an M3D layout [14], which reduces L1 cache latency and planar footprint by 41% and 44%, respectively.

6.1.2 Pipeline Width. To design wider pipelines, first, we increase the width and depth of the pipeline SRAM structures (e.g., L/SQ, ROB), leading to an 11.6% area overhead per core (7.8% of the logic area). By exploiting the multi-layer SRAM structure supported by M3D [14, 54], we increase the size of these structures without increasing their latency and affecting the pipeline frequency. Second, we increase the width of the decode structure and the functional units. Doubling the number of decode structures and functional units (including six integer ALUs, one FPU, and one complex ALU) leads to a 16.5% area overhead *per core* (11.2% of the logic area).¹⁰ We exploit part of the extra die area freed up due to removing the L2 cache to double the number of decode and execution units.

6.1.3 Register File-Level Synchronization. To facilitate high thread-level parallelism, we introduce a new fine-grained synchronization technique, using M3D’s dense inter-layer connectivity, to improve inter-thread communication. We use the thin ILVs between the logic layers in the M3D system to perform fine-grained inter-thread communication in the register file (RF) instead of the memory hierarchy. The thin ILVs enable increasing the bandwidth of the SRAM cells in the RF by adding extra access transistors to each cell. The short ILVs can efficiently connect the extra access transistors in a secondary logic layer to the SRAM cells located on the primary layer, without increasing the RF latency. RevaMp3D leverages this to add extra ports to the RF of each core and uses the extra ports for fine grained inter-thread communication. Fig. 18 shows how fine-grained ILVs can add additional access ports to an SRAM cell to increase bandwidth. *Small diameter* and *vertical* connections are essential for adding extra ports efficiently. Due to the small ILV diameter, adding vertical ports increases the SRAM cell area at the 15nm technology node by less than 0.1% [14]. However, for vertical connections with much larger diameters (e.g., $2.6\mu\text{m}$ TSVs), this overhead increases significantly [14]. For horizontal connections (i.e., in 2D), adding extra ports leads to not only area overhead, but also an increased lateral delay for accessing the port.

¹⁰We use McPAT [112] in 22nm technology for area analysis. Even though the absolute area values of the logic components in our CNFET-based M3D baseline do not equal the values generated by McPAT, we are interested in the area *ratio* of different logic components.

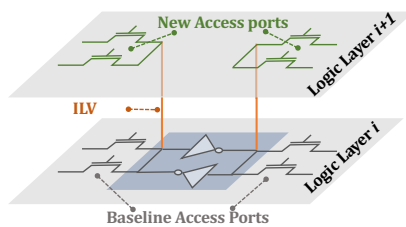


Fig. 18. Vertical layout for extra ports.

Due to RF’s limited size, we only leverage it for communications that involve small data, such as synchronization. While RF-level communication has been proposed in prior work [113], the adoption of such proposals is challenging in 2D or 3D systems due to the limitations of adding extra ports to the RFs. Without adding extra ports, the synchronization operations need to compete with the pipeline’s register operand accesses for the limited RF ports.

To enable fine-grained locking, where one lock variable is associated with a small amount of application data, each core writes the address of the data that is being locked by the core to other cores’ RF (instead of using lock variables updated through the cache hierarchy and the coherence protocol). Fig. 19 shows an overview of this process. When a core wants to send a lock variable (1 in Fig. 19), it can use the baseline interconnects (in this case, a meshes-of-trees network, same as the baseline M3D system), but instead of sending data to the memory hierarchy, it sends it to the register file of the other cores (2). To this end, the router nodes need a simple selection structure (3) to determine whether data needs to go through the baseline path to the memory hierarchy or to go through the synchronization path.

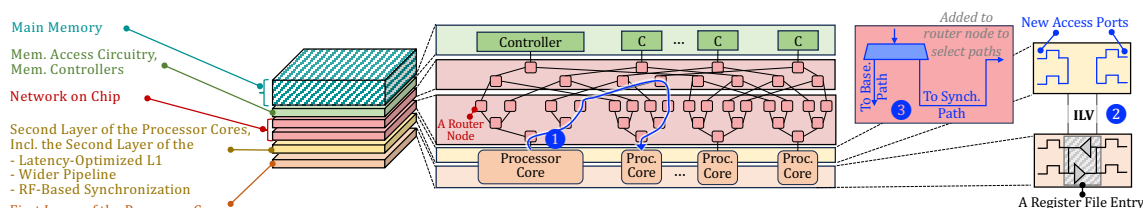


Fig. 19. The overview of the register file-level synchronization.

Fig. 20 shows the speedup of RF synchronization (RF-sync) compared to the baseline (Base-sync) for the synchronization microbenchmarks. We observe on average 1.78× and up to 2.31× speedup over the M3D-based system with the baseline coherence-based synchronization.

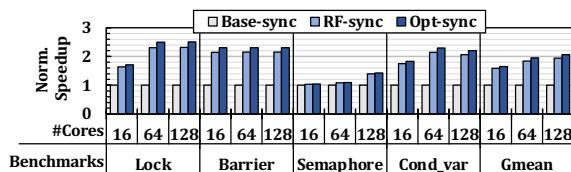


Fig. 20. Speedup of the register file-level synchronization.

Area and Timing Implications. In fine-grained locking schemes of real workloads, prior works [110, 114] show that the number of synchronization variables that are active at any given time during the execution is small (typically up to 4 variables). Thus, there is no need for large additional space in the RF. RF takes 0.2% of the logic area in our baseline. Therefore, the planar area overhead of adding extra ports to 4 entries of the RF is less than 0.001% of the logic area.

Since the extra ports are connected to RF entries from another logic layer using the short ILVs, they do not change the structure and timing of the RF accesses for the baseline core operations.

Security Implications. This technique does not exacerbate the security guarantees compared to the baseline system due to two reasons. First, we propose this technique for threads that are from the same multi-threaded application (with a similar protection domain and from one user). Therefore, threads from different applications, users, or protection domains do not access each other’s data in the register file for synchronization. Second, threads spawned from one application already exchange data through the cache coherence protocol, which has already led to multiple attacks that leverage the coherence traffic to establish side channels. We conclude that utilizing the register file for synchronization does not open up new attack surfaces and does not exacerbate the existing security issues with data coherence.

6.2 Leveraging M3D Memory Layers

We propose a new processor frontend design that memoizes the repetitive fetched, decoded, and re-ordered μ ops, stores them in M3D main memory, and turns off the relevant parts of the core pipeline when the same μ ops execute in a loop. The high-bandwidth, energy-efficient M3D memory enables storing and loading the memorized instructions efficiently. This addresses two key bottlenecks that we identify in the M3D baseline. First, it can alleviate the shifted M3D system’s energy bottlenecks that are dominated by the processor core’s energy consumption. As programmers commonly use loops in their codes, a significant number of instructions in programs are typically repeated [64, 65, 115]. Therefore, turning off the fronted and reordering structures can lead to energy saving by eliminating a significant portion of the average energy per core in the baseline OoO core. Second, this technique alleviates the speculation bottleneck in the M3D system by reducing the pipeline fill latency and number of pipeline bubbles in the event of branch misprediction since the instructions do not need to be fetched, decoded, and reordered if they are already memoized.

While prior works [64, 115] have also explored μ op memorization with an Execution Cache (EC), these works leverage SRAM caches that incur large area overheads. However, RevaMp3D leverages the high-bandwidth connection between logic and memory layers as a unique opportunity provided by M3D integration, and stores the memorized μ ops in the main memory. Prior work [64] shows that to fully benefit from μ op memoization, we need a large on-chip EC (e.g., up to 100KB) per core, which incurs high area overheads, occupying 15% of the logic area of the baseline processor core. Considering a fixed area budget, this overhead can come at the cost of key core components and, therefore, sacrifice performance. Some prior works propose a smaller EC for area efficiency but at the cost of memoizability opportunities in applications with a large instruction footprint and large loops [64, 115–117]. In contrast, using M3D main memory for storing the memorized μ ops paves the way for architecting a large and scalable EC at low area cost. We use a small buffer to store the prefetched memoized μ ops from main memory and provide a one-cycle access latency.

Fig. 21 demonstrates Energy per Instruction (EPI) in (1) no memization (No-Memo), (2) memoizing μ ops in a 100KB-SRAM EC (Baseline-Memo), and (3) memoizing μ ops in M3D main memory (M3D-Memo). In (2) and (3), the frontend, decode, and reordering structures are power-gated when the memoized μ ops execute. We break down the EPI to the energy spent on the core, the SRAM-based EC (Cache-EC) in Baseline-Memo, and the main memory-based EC (M3D-EC) and the small buffer (Buffer-EC) in M3D-Memo. We observe that M3D-Memo reduces EPI by 37% over No-Memo and achieves comparable EPI compared to Baseline-Memo, while incurring significantly lower area cost.

Implementation. We implement M3D-Memo based on prior work [64] that proposes an SRAM-based EC. As shown in Fig. 22, we place the *Memoization Unit (MU)* after the issue stage. Note that the MU does not add an extra stage to the pipeline since instructions are issued to the execution stage and the MU in parallel. We use the high main memory bandwidth in M3D to memoize both the taken and not-taken paths of hard-to-predict branches. The MU has three main

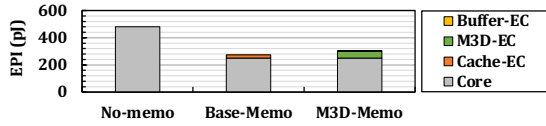


Fig. 21. Energy per instruction of three design points.

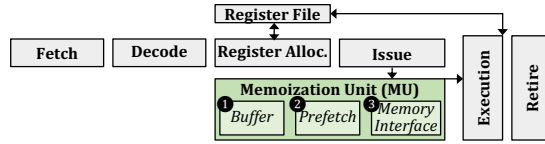
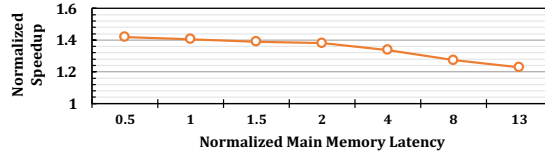


Fig. 22. RevaMp3D's Memoization Unit.

components: ❶ a small 1.28KB SRAM buffer to provide one-cycle access latency to the memoized μ ops, ❷ a simple stride prefetcher that reads μ ops from the main memory and fills the buffer to hide the memory access latency, and ❸ a memory interface that uses two read/write ports for the taken and not-taken paths and an address bus. We calculate the area of the MU unit using Synopsys Design Compiler and show that it occupies less than 5% of the L1 cache area. We use a preserved address space to store the memoized μ ops.

Performance Implications. M3D-Memo improves the performance of speculation-bound workloads by reducing pipeline fill latency and bubbles. However, M3D-Memo *limits* renaming each architectural register to a specific register pool (similar to [64]), which can negatively affect performance. Overall, the effect of reducing pipeline depth and fill latency in the M3D-based system outweighs this overhead, leading to up to 35.5% speedup for speculation-bound workloads and a modest average speedup of 1.4% across all evaluated workloads.

To demonstrate the impact of this design as the M3D memory latency changes, Fig. 23 shows the performance of a 64-core M3D system with the main memory-based μ op memorization for a speculation-bound workload (Tri). Performance at each point is normalized against the baseline M3D system with that memory latency. In all configurations, the M3D system has the same bandwidth. We find that the main memory-based μ op memoization achieves significant speedups (22–42%) across a range of memory latencies, with particularly larger gains at lower latency values.

Fig. 23. Performance impact of the μ op memoization technique on M3D-based systems with different memory latency values.

7 End-to-End Evaluation

7.1 End-to-End Speedup

Fig. 24 (a) shows the speedup of RevaMp3D (with all design decisions of §6) over the state-of-the-art M3D system, across all multi-threaded workloads and the multi-programmed workload mixes. Each data point shows the speedup of the optimized M3D with N cores over the baseline M3D with N cores, where $N \in \{1, 16, 64, 128\}$. We make two observations. First, we observe a significant performance improvement, on average 79.4% and 67.6% speedups across all

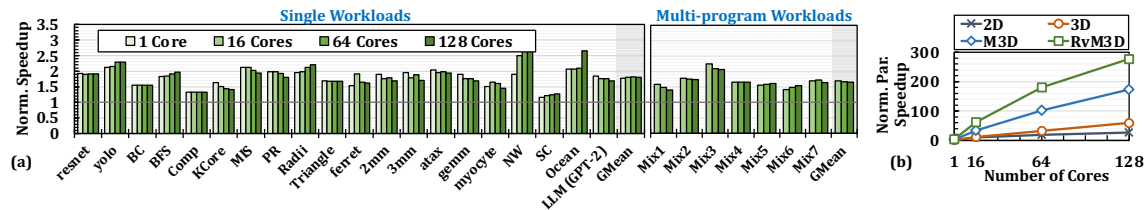


Fig. 24. RevaMp3D's Speedup over (a) the M3D baseline, and (b) the 2D and 3D baselines on average across all evaluated workloads.

core counts for multi-threaded workloads and multi-programmed workload mixes, respectively. Second, the suggested design decisions improve the performance of *all evaluated workloads* (i.e., no workload suffers from slowdown).

Fig. 24 (b) shows RevaMp3D’s speedup, averaged across all evaluated workloads, over the state-of-the-art 2D, 3D, and M3D-based systems. We observe that RevaMp3D provides significant benefits, resulting in 7.14 \times and 4.96 \times speedups over the 2D and 3D systems, respectively, further increasing the potential performance benefits of M3D integration.

For varying main memory latency values, Fig. 25 shows the distribution of the end-to-end speedup of RevaMp3D over the baseline M3D-based system across all the workloads. RevaMp3D’s speedup at each memory latency point is reported relative to the performance of the baseline system at that same latency. Both RevaMp3D and baseline feature 64 cores. We observe that RevaMp3D provides speedup for all evaluated workloads even when memory latency increases to 2 \times larger, while some workloads exhibit slowdowns at higher latencies. This is because, as shown in Fig. 9, some design decisions in RevaMp3D are primarily tailored for smaller latency values. While not all RevaMp3D design choices lead to speedup for M3D-based systems with high latency, the high-bandwidth connectivity between logic and memory layers in the M3D-based system can still provide several benefits (e.g., RF-based inter-thread synchronization and the efficient μ op memorization), which provide benefits for M3D-based systems different memory latency values. Therefore, depending on the configuration of the M3D-based system and its main memory characteristics, different subsets of RevaMp3D’s design decisions can be adopted to enhance both performance and energy efficiency.

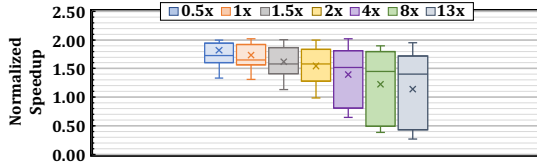


Fig. 25. RevaMp3D’s speedup with various memory latencies.

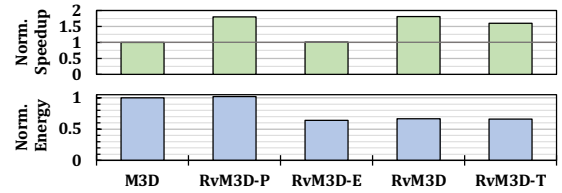


Fig. 26. Speedup and energy of RevaMp3D’s configurations.

7.2 Analysis of Different RevaMp3D Configurations

We evaluate the benefits of four different RevaMp3D configurations, each optimized for different goals. Fig. 26 shows the normalized speedup and energy consumption of each configuration relative to the baseline M3D system, averaged across all evaluated workloads. First, RvM3D-P represents the RevaMp3D configuration that only applies the performance-improving design decisions in §6.1. Second, RvM3D-E represents the configuration that only applies the design decisions in §6.2, with the main goal of reducing energy. Third, RvM3D combines both sets of design decisions. Fourth, RvM3D-I represents a low-frequency implementation of RevaMp3D that is iso-power with the M3D baseline. We make four observations. First, RvM3D-P leads to similar average energy consumption compared to the M3D baseline (with only a modest 2% increase). This is because, given the high energy efficiency of the M3D main memory, removing L2 does not lead to a significant increase in energy. Furthermore, increasing the width of the pipeline SRAM structures using the M3D vertical layout [14] does not increase their energy per access since their overall planar wire length does not increase. Second, RvM3D-E leads to 36.6% lower average energy consumption since, for each of our workloads, we observe a high degree of memoizability, where at least 99% of their dynamic instructions follow the same schedule. RvM3D-E leads to an average speedup of 1.4%. Third, RvM3D leads to an 80.6% average speedup. While the performance-improving design decisions lead to an 84% power increase over the baseline M3D, the memoization technique allows this improvement at only 18% higher power consumption. Fourth, RvM3D-I outperforms the 4GHz baseline M3D by 60.5%, without an increase in power consumption. We conclude that our approach increases the M3D system’s performance per Watt by both improving performance and lowering energy consumption.

7.3 Overall Area Reduction

We summarize the area impact of RevaMp3D in Table 5. We observe an *overall* 12.3% area reduction compared to the baseline M3D-based system. The freed-up area can be used to further improve performance (e.g., by adding more cores). RevaMp3D re-purposes the logic layer used for the L2 cache in the baseline M3D-based system (shown in Fig. 2) to add all the needed components (e.g., the extra RF ports, the second layer of the L1 cache, and the second layer of the wider pipeline’s SRAM structures and its additional functional units), while consuming smaller logic area than the L2 cache.

Table 5. Area Impact of RevaMp3D.

Proposed Change	Area Impact (% of logic area)
L2 cache removal	-32%
Wider pipeline	+19%
EC Buffer	+0.7%
Register file overheads	< +0.01%
Total	-12.3%

8 Discussion

Scaling Data Size Beyond Main Memory Capacity. While a system with a single M3D chip can potentially provide hundreds of gigabytes of main memory [7, 9], for even larger requirements, a system can employ multiple M3D chips. In that case, off-chip access costs more overhead than on-chip access, and techniques that alleviate the remote access overhead using scheduling, data placement, replication, or migration can be orthogonally applied [71, 118, 119]. Advances in integration technology can further reduce the cost of off-chip accesses in M3D by enabling the monolithic integration of *multiple* M3D stacks [120].

Hardware/Software Co-Design. Memory bottleneck affects both hardware and software in today’s systems. This work explores the implications of M3D on the hardware design of cores and caches. We believe that it is essential to also revisit the software stack to better leverage the underlying M3D hardware. In the operating systems, memory management and process management units can be revisited to be aware of M3D’s trade-offs. In our work, we considered 2MB page sizes. Based on our analysis with Virtuoso [121], a state-of-the-art framework for the software and hardware components of the virtual memory subsystem, we observe that in our M3D baseline, using the 2MB page size leads to 5.7% average speedup across our evaluated workloads compared to using the 4KB page size. We believe further detailed analysis of the system software stack in the context of the M3D technology would be an important direction to explore and we hope our analysis of new bottlenecks and opportunities of M3D systems guides future hardware/software co-design efforts for this technology.

9 Related Work

To our knowledge, this is the first work to re-examine the processor core and cache hierarchy based on rigorous bottleneck analysis of a wide range of workloads and the new trade-offs imposed by M3D integration.

Device and Circuit-Level Integration. Many works (e.g., [34–42, 122–129]) focus on the design of efficient M3D devices with respect to performance, power, energy, area, temperature, yield and reliability. Other studies show the benefits of M3D technology in comparison to 3D-stacked technologies [43, 44]. Several works (e.g., [3, 10, 45]) study M3D physical integration and layout. Several works explore heterogeneous device layers in M3D (e.g., [46–49, 130]).

Designing M3D Processors. Recent works propose 3D partitioning techniques for logic-only M3D processors (e.g., [14, 50, 51]) to improve the latency of different components by decreasing their wire lengths. Other works show how to leverage M3D to design efficient SRAMs (e.g., [53–56]) or NoCs (e.g., [50, 52]). Some works (e.g., [3, 52]) discuss the memory system challenges, such as optimizing the memory array structures and developing techniques to increase

memory parallelism (e.g., SIMD units and non-blocking loads). Some works explore the benefits of M3D integration of non-volatile memory on top of last-level caches and how to design the interface between them (e.g., [3, 6, 10]). While prior works propose various optimizations, we analyze the implications of M3D on (i) the real-world application bottlenecks and (ii) architectural designs that have been conventionally specialized to tackle the memory bottleneck. For example, while prior works propose optimizations to caches in M3D [9, 14], we show that such optimizations are *not essential* beyond L1 for M3D-based systems with low memory latency values.

Accelerating Specific Applications. Various works (e.g., [51, 57–63, 131–134]) design domain-specific accelerators in M3D. Some works (e.g., [135]) suggest M3D FPGAs. While our work focuses on general-purpose systems, we hope that our design choices can also inspire domain-specific systems.

Processing-Using-Memory in M3D-based systems. Some works (e.g., [130, 136, 137]) design processing-using-memory systems specialized for M3D-integrated systems.

3D Caches. Prior works propose 3D caches to achieve low latency and high bandwidth, such as AMD’s 3D SRAM V-Cache [138] and SILO [139]. However, due to their limited capacity, they cannot fully address main memory bottlenecks.

10 Conclusion

In this work, we design the processor core and cache hierarchy, given the fundamentally new trade-offs of M3D. We show that for a variety of workloads on a state-of-the-art M3D system, the performance and energy bottlenecks substantially shift from the main memory to the processor core and cache hierarchy, emphasizing the need to revisit current designs. We conduct a rigorous design space exploration of the key components of the processor core and cache hierarchy to understand the implications of the M3D system’s shifted bottlenecks on their design. Based on these implications and by taking advantage of the new opportunities of M3D integration, we design a new M3D system, RevaMp3D. We show that RevaMp3D provides significant performance improvement and energy reduction while achieving a smaller logic area compared to the state-of-the-art M3D system.

References

- [1] T Srimani, A Bechdolt, et al. N3XT 3D Technology Foundations and Their Lab-to-Fab: Omni 3D Logic, Logic+ Memory Ultra-Dense 3D, 3D Thermal Scaffolding. In *IEDM*, 2023.
- [2] Max M Shulaker, Gage Hills, et al. Carbon nanotube computer. *Nature*, 2013.
- [3] Candace Walden, Devesh Singh, et al. Monolithically Integrating Non-Volatile Main Memory over the Last-Level Cache. *ACM TACO*, 2021.
- [4] Subir Ghosh, Yikai Zheng, et al. Monolithic and heterogeneous three-dimensional integration of two-dimensional materials with high-density vias. *Nature Electronics*, 2024.
- [5] Max Shulaker, Tony Wu, et al. Monolithic 3D Integration of Logic and Memory: Carbon Nanotube FETs, Resistive RAM, and Silicon FETs. In *IEDM*, 2014.
- [6] Meenatchi Jagasivamani, Candace Walden, et al. Tileable monolithic reram memory design. In *COOL CHIPS*, 2020.
- [7] Max Shulaker, Gage Hills, et al. Three-dimensional integration of nanotechnologies for computing and data storage on a single chip. *Nature*, 2017.
- [8] Mohamed M Sabry Aly, Mingyu Gao, et al. Energy-efficient abundant-data computing: The N3XT 1,000 x. *Computer*, 2015.
- [9] Mohamed M Sabry Aly, Tony F Wu, et al. The N3XT Approach to Energy-Efficient Abundant-Data Computing. *IEEE*, 2018.
- [10] Meenatchi Jagasivamani, Candace Walden, et al. Analyzing the Monolithic Integration of a ReRAM-based Main Memory into a CPU’s Die. *IEEE Micro*, 2019.
- [11] Yuanqing Cheng, Xiaochen Guo, and Vasilis F Pavlidis. Emerging monolithic 3d integration: Opportunities and challenges from the computer system perspective. *Integration*, 2022.
- [12] NVidia. NVIDIA A100 Tensor Core GPU Architecture, 2020. <https://www.nvidia.com/en-us/data-center/a100/>.
- [13] SK Hynix. Fastest DRAM with enhanced heat dissipation, 2021. <https://product.skhynix.com/products/dram/hbm/hbm2e.go>.
- [14] Bhargava Gopireddy and Josep Torrellas. Designing Vertical Processors in Monolithic 3D. In *ISCA*, 2019.
- [15] Soon-Wook Kim, Mikael Detalle, et al. Ultra-fine pitch 3d integration using face-to-face hybrid wafer bonding combined with a via-middle through-silicon-via process. In *ECTC*, 2016.
- [16] Dimin Niu, Shuangchen Li, et al. 184QPS/W 64Mb/mm² 3D logic-to-DRAM hybrid bonding with process-near-memory engine for recommendation system. In *ISSCC*, 2022.

- [17] Bai Fujun, Jiang Xiping, et al. A stacked embedded DRAM array for LPDDR4/4X using hybrid bonding 3D integration with 34GB/s/1Gb 0.88 pJ/b logic-to-memory interface. In *IEDM*, 2020.
- [18] L. Arnaud, C. Karam, et al. Three-dimensional hybrid bonding integration challenges and solutions toward multi-wafer stacking. *MRS communications*, 2020.
- [19] Han-Wen Hu and Kuan-Neng Chen. Development of low temperature CuCu bonding and hybrid bonding for three-dimensional integrated circuits (3D IC). *Microelectronics Reliability*, 2021.
- [20] Theodros Nigussie, Tse-Han Pan, et al. Design benefits of hybrid bonding for 3D integration. In *ECTC*, 2021.
- [21] Yiwei Du, Jianshi Tang, et al. Monolithic 3d integration of analog rram-based computing-in-memory and sensor for energy-efficient near-sensor computing. *Advanced Materials*, 2024.
- [22] Chanseul Lee, Sunbum Kim, et al. Heterogeneous monolithic 3D integration for hybrid vertical CMOS inverter using n-type IGTO TFT on p-type Si FET. *Materials Science in Semiconductor Processing*, 2025.
- [23] Zhenyu Wang, Pragnya Sudershan Nalla, et al. HISIM: Analytical Performance Modeling and Design Space Exploration of 2.5 D/3D Integration for AI Computing. *IEEE Transactions on Computer-Aided Design of Integrated Circuits and Systems*, 2025.
- [24] Ali Sedaghatgoo, Amir M Hajisadeghi, et al. ARMAN: A Reconfigurable Monolithic 3D Accelerator Architecture for Convolutional Neural Networks. *arXiv*, 2024.
- [25] Kyungwook Chang and Sung Kyu Lim. Design and tool solutions for monolithic three-dimensional integrated circuits. In *Handbook of Computer Architecture*. 2024.
- [26] Sai Pentapati and Sung-Kyu Lim. Heterogeneous Monolithic 3-D IC Designs: Challenges, EDA Solutions, and Power, Performance, Cost Tradeoffs. *TVLSI*, 2024.
- [27] Jinwoo Kim, Lingjun Zhu, et al. A PPA study for heterogeneous 3-D IC options: Monolithic, hybrid bonding, and microbumping. *TVLSI*, 2023.
- [28] SkyWater. SkyWater Technology Foundry Selects Veeco's Waferstorm for 3D Monolithic System-on-a-Chip Development. <https://www.skywatertechnology.com/skywater-technology-foundry-selects-veeco-waferstorm-for-3d-monolithic-system-on-a-chip-development/>.
- [29] S Liao, L Yang, et al. Complementary Field-Effect Transistor (CFET) Demonstration at 48nm Gate Pitch for Future Logic Technology Scaling. In *IEDM*, 2023.
- [30] S Subramanian, M Hosseini, et al. First monolithic integration of 3d complementary fet (cfet) on 300mm wafers. In *IEEE Symposium on VLSI Technology*, 2020.
- [31] Ki Seok Kim, Seunghwan Seo, et al. Growth-based monolithic 3D integration of single-crystal 2D semiconductors. *Nature*, 2024.
- [32] S. Subramanian, M. Hosseini, et al. First Monolithic Integration of 3D Complementary FET (CFET) on 300mm Wafers. In *IEEE Symposium on VLSI Technology*, 2020.
- [33] FF Athena, E Ambrosi, et al. First demonstration of an np oxide semiconductor complementary gain cell memory. In *IEDM*, 2024.
- [34] Bon Woong Ku, Peter Debacker, et al. Physical design solutions to tackle FEOL/BEOL degradation in gate-level monolithic 3D ICs. In *ISLPED*, 2016.
- [35] Chang Liu and Sung Kyu Lim. A design tradeoff study with monolithic 3d integration. In *ISQED*, 2012.
- [36] Shreepad Panth, Sandeep Samal, et al. Design challenges and solutions for ultra-high-density monolithic 3d ics. In *S3S*, 2014.
- [37] Kyungwook Chang, Abhishek Koneru, et al. Design automation and testing of monolithic 3D ICs: Opportunities, challenges, and solutions. In *ICCAD*, 2017.
- [38] Sandeep Kumar Samal, Shreepad Panth, et al. Fast and Accurate Thermal Modeling and Optimization for Monolithic 3D ICs. In *DAC*, 2014.
- [39] Prachi Shukla, Ayse K Coskun, et al. An overview of thermal challenges and opportunities for monolithic 3d ics. In *GLSVLSI*, 2019.
- [40] Dongjin Lee, Sourav Das, et al. Performance and thermal tradeoffs for energy-efficient monolithic 3d network-on-chip. *TODAES*, 2018.
- [41] Sandeep Kumar Samal, Kambiz Samadi, et al. Full chip impact study of power delivery network designs in monolithic 3d ics. In *ICCAD*, 2014.
- [42] Melanie Brocard, Benoit Mathieu, et al. Transistor temperature deviation analysis in monolithic 3D standard cells. In *ISVLSI*, 2017.
- [43] Sandeep Kumar Samal, Deepak Nayak, et al. Monolithic 3d ic vs. tsv-based 3d ic in 14nm finfet technology. In *S3S*, 2016.
- [44] Deepak Kumar Nayak, Srinivasa Banna, et al. Power, performance, and cost comparisons of monolithic 3d ics and tsv-based 3d ics. In *S3S*, 2015.
- [45] Meenatchi Jagasivamani, Candace Walden, et al. Design for rram-based main-memory architectures. In *MEMSYS*, 2019.
- [46] Farzaneh Zokaee, Mingzhe Zhang, et al. Magma: A monolithic 3D vertical heterogeneous ReRAM-based main memory architecture. In *DAC*, 2019.
- [47] Gauthaman Murali, Xiaoyu Sun, et al. Heterogeneous mixed-signal monolithic 3-D in-memory computing using resistive RAM. *TVLSI*, 2020.
- [48] Anwasha Chatterjee, Shouvik Musavvir, et al. Power Management of Monolithic 3D Manycore Chips with Inter-tier Process Variations. *JETC*, 2021.
- [49] Gauthaman Murali and Sung Kyu Lim. Heterogeneous 3D ICs: Current Status and Future Directions for Physical Design Technologies. In *DATE*, 2021.
- [50] Dylan Stow, Itir Akgun, et al. Efficient System Architecture in the Era of Monolithic 3D: Dynamic Inter-tier Interconnect and Processing-in-Memory. In *DAC*, 2019.
- [51] Biresh Kumar Joardar, Aqeeb Iqbal Arka, et al. 3D++: Unlocking the Next Generation of High-Performance and Energy-Efficient Architectures using M3D Integration. In *DATE*, 2021.
- [52] Meenatchi Jagasivamani, Candace Walden, et al. Memory-systems challenges in realizing monolithic computers. In *MEMSYS*, 2018.
- [53] Srivatsa Srinivasa, Akshay Krishna Ramanathan, et al. A monolithic-3d sram design with enhanced robustness and in-memory computation support. In *ISLPED*, 2018.
- [54] Srivatsa Srinivasa, Wei-Hao Chen, et al. Monolithic-3D integration augmented design techniques for computing in SRAMs. In *ISCAS*, 2019.

- [55] Srivatsa Srinivasa, Yung-Ning Tu, et al. Monolithic 3D+-IC based reconfigurable compute-in-memory SRAM macro. In *Symposium on VLSI Technology*, 2019.
- [56] Joonho Kong, Young-Ho Gong, and Sung Woo Chung. Architecting large-scale SRAM arrays with monolithic 3D integration. In *ISLPED*, 2017.
- [57] Abdallah M. Felfl, Kamalika Datta, et al. Quantifying the Benefits of Monolithic 3D Computing Systems Enabled by TFT and RRAM. In *DATE*, 2020.
- [58] Ye Yu and Niraj K Jha. Spring: A sparsity-aware reduced-precision monolithic 3d cnn accelerator architecture for training and inference. *IEEE TETC*, 2020.
- [59] Sho Ko, Yun Joon Soh, and Jishen Zhao. Efficient Implementation of Multi-Channel Convolution in Monolithic 3D ReRAM Crossbar. *arXiv*, 2020.
- [60] Yu Huang, Long Zheng, et al. RAGra: Leveraging monolithic 3D ReRAM for massively-parallel graph processing. In *DATE*, 2019.
- [61] Muhammad Abdullah Hanif, Aditya Manglik, and Muhammad Shafique. Resistive crossbar-aware neural network design and optimization. *IEEE Access*, 2020.
- [62] Tony Wu, Haitong Li, et al. Brain-inspired computing exploiting carbon nanotube fets and resistive ram: Hyperdimensional computing case study. In *ISSCC*, 2018.
- [63] Tony F Wu, Haitong Li, et al. Hyperdimensional computing exploiting carbon nanotube FETs, resistive RAM, and their monolithic 3D integration. *IEEE Journal of Solid-State Circuits*, 2018.
- [64] Emil Talpes and Diana Marculescu. Execution cache-based microarchitecture for power-efficient superscalar processors. *TVLSI*, 2005.
- [65] Baruch Solomon, Avi Mendelson, et al. Micro-operation cache: A power aware frontend for variable instruction length isa. *TVLSI*, 2003.
- [66] Daniel Sanchez and Christos Kozyrakis. ZSim: Fast and Accurate Microarchitectural Simulation of Thousand-Core Systems. In *ISCA*, 2013.
- [67] Geraldo F Oliveira, Juan Gómez-Luna, et al. Damov: A new methodology and benchmark suite for evaluating data movement bottlenecks. *IEEE Access*, 2021.
- [68] Santhosh Srinath, Onur Mutlu, et al. Feedback Directed Prefetching: Improving the Performance and Bandwidth-Efficiency of Hardware Prefetchers. In *HPCA*, 2007.
- [69] Makoto Motoyoshi. Through-Silicon Via (TSV). *Proceedings of the IEEE*, 2009.
- [70] Onur Mutlu, Saugata Ghose, et al. A Modern Primer on Processing in Memory. *Emerging Computing: From Devices to Systems - Looking Beyond Moore and Von Neumann*, 2021.
- [71] J. Ahn, S. Hong, et al. A Scalable Processing-in-memory Accelerator for Parallel Graph Processing. In *ISCA*, 2015.
- [72] Amirali Boroumand, Saugata Ghose, et al. Google Workloads for Consumer Devices: Mitigating Data Movement Bottlenecks. In *ASPLOS*, 2018.
- [73] Amirali Boroumand, Saugata Ghose, et al. CoNDA: Efficient Cache Coherence Support for Near-Data Accelerators. In *ISCA*, 2019.
- [74] Kevin Hsieh, Samira Khan, et al. Accelerating Pointer chasing in 3D-stacked Memory: Challenges, Mechanisms, Evaluation. In *ICCD*.
- [75] Ravi Nair, Samuel F Antao, et al. Active Memory Cube: A Processing-in-memory Architecture for Exascale Systems. *IBM Journal of Research and Development*, 2015.
- [76] Lifeng Nai, Ramyad Hadidi, et al. GraphPIM : Enabling Instruction-Level PIM Offloading in Graph Computing Frameworks. In *HPCA*, 2017.
- [77] Seongguk Kim, Subin Kim, et al. Signal Integrity and Computing Performance Analysis of a Processing-In-Memory of High Bandwidth Memory (PIM-HBM) Scheme. *IEEE Transactions on Components, Packaging and Manufacturing Technology*, 2021.
- [78] Lingjun Zhu, Lennart Bamberg, et al. High-performance logic-on-memory monolithic 3-D IC designs for arm Cortex-A processors. *TVLSI*, 2021.
- [79] Yijun Li, Jianshi Tang, et al. Monolithic 3D integration of logic, memory and computing-in-memory for one-shot learning. In *IEDM*, 2021.
- [80] Akifumi Kawahara, Ryotaro Azuma, et al. An 8 mb multi-layered cross-point reram macro with 443 mb/s write throughput. *IEEE Journal of Solid-State Circuits*, 2012.
- [81] Chung-Cheng Chou, Zheng-Jun Lin, et al. An N40 256K× 44 embedded RRAM macro with SL-precharge SA and low-voltage current limiter to improve read and write performance. In *ISSCC*, 2018.
- [82] Bryan Black, Murali Annavaram, et al. Die Stacking (3D) Microarchitecture. In *MICRO*, 2006.
- [83] Jongman Kim, Chrysostomos Nicopoulos, et al. A novel dimensionally-decomposed router for on-chip communication in 3D architectures. In *ISCA*, 2007.
- [84] Vasilis F Pavlidis and Eby G Friedman. 3-D topologies for networks-on-chip. *TVLSI*, 2007.
- [85] Mindy Bishop, Gage Hills, et al. Fabrication of carbon nanotube field-effect transistors in commercial silicon manufacturing facilities. *Nature Electronics*, 2020.
- [86] Devesh Singh and Donald Yeung. MORSE: Memory Overwrite Time Guided Soft Writes to Improve ReRAM Energy and Endurance. In *PACT*, 2024.
- [87] Andrew M Bartolo, Mohamed M Sabry Aly, et al. MC-ELMM: Multi-Chip Endurance-Limited Memory Management. In *MEMSYS*, 2023.
- [88] Joseph Redmon. Darknet: Open Source Neural Networks in C. <http://pjreddie.com/darknet>, 2013.
- [89] Julian Shun and Guy E Blelloch. Ligra: A Lightweight Graph Processing Framework for Shared Memory. In *PPoPP*, 2013.
- [90] Shuai Che, Michael Boyer, et al. Rodinia: A Benchmark Suite for Heterogeneous Computing. In *IISWC*, 2009.
- [91] Steven Cameron Woo, Moriyoshi Ohara, et al. The SPLASH-2 Programs: Characterization and Methodological Considerations. *ISCA*, 1995.
- [92] Louis-Noël Pouchet. Polybench: The Polyhedral Benchmark Suite. URL: <http://www.cs.ucla.edu/pouchet/software/polybench>, 2012.
- [93] Christian Bienia, Sanjeev Kumar, et al. The PARSEC Benchmark Suite: Characterization and Architectural Implications. In *PACT*, 2008.
- [94] Geraldo F. Oliveira, Juan Gómez-Luna, et al. DAMOV: A New Methodology and Benchmark Suite for Evaluating Data Movement Bottlenecks.
- [95] Ahmad Yasin. A Top-Down Method for Performance Analysis and Counters Architecture. In *ISPASS*, 2014.
- [96] Svilen Kanev, Juan Pablo Darago, et al. Profiling a Warehouse-Scale Computer. In *ISCA*, 2015.

- [97] Utku Sirin, Ahmad Yasin, and Anastasia Ailamaki. A Methodology for OLTP Micro-Architectural Analysis. In *DAMON*, 2017.
- [98] R. Appuswamy, J. Fellay, and N. Chaturvedi. Sequence Alignment Through the Looking Glass. In *IPDPSW*, 2018.
- [99] Intel. Intel VTune Amplifier 2019 User Guide, 2018. <https://software.intel.com/en-us/vtune-amplifier-help>.
- [100] S. Ghose, T. Li, et al. Demystifying Complex Workload-DRAM Interactions: An Experimental Study. In *SIGMETRICS*, 2020.
- [101] Vikram Sharma Mailthody, Zaid Qureshi, et al. Deepstore: In-storage acceleration for intelligent queries. In *MICRO*, 2019.
- [102] Po-An Tsai, Changping Chen, and Daniel Sanchez. Adaptive Scheduling for Systems with Asymmetric Memory Hierarchies. In *MICRO*, 2018.
- [103] Tse-Yu Yeh and Yale N Patt. Two-level adaptive training branch prediction. In *MICRO*, 1991.
- [104] André Seznec. Targe-sc-1 branch predictors again. In *JILP Workshop on Computer Architecture Competitions: Championship Branch Prediction*, 2016.
- [105] Jack Choquette, Wishwesh Gandhi, et al. NVIDIA A100 Tensor Core GPU: Performance and Innovation. *IEEE Micro*, 2021.
- [106] Aydin O Balkan, Gang Qu, and Uzi Vishkin. Mesh-of-trees and alternative interconnection networks for single-chip parallelism. *TVLSI*, 2009.
- [107] Jacob Benesty, Jingdong Chen, et al. Pearson correlation coefficient. In *Noise reduction in speech processing*. 2009.
- [108] Taeho Kgil, Shaun D'Souza, et al. PicoServer: using 3D stacking technology to enable a compact energy efficient chip multiprocessor. In *ASPLOS*, 2006.
- [109] Taeho Kgil, Ali Saidi, et al. PicoServer: Using 3D stacking technology to build energy efficient servers. *JETC*, 2008.
- [110] Tudor David, Rachid Guerraoui, and Vasileios Trigonakis. Everything you always wanted to know about synchronization but were afraid to ask. In *SOSP*, 2013.
- [111] Tudor David. Libslock. URL: <https://github.com/tudordavid/libslock>.
- [112] Sheng Li, Jung Ho Ahn, et al. McPAT: An integrated power, area, and timing modeling framework for multicore and manycore architectures. In *MICRO*, 2009.
- [113] Stephen Keckler, William Dally, et al. Exploiting fine-grain thread level parallelism on the MIT multi-ALU processor. *ACM SIGARCH Computer Architecture News*, 1998.
- [114] Christina Giannoula, Nandita Vijaykumar, et al. Synchron: Efficient synchronization support for near-data-processing architectures. In *HPCA*, 2021.
- [115] Emil Talpes and Diana Marculescu. Power reduction through work reuse. In *ISLPED*, 2001.
- [116] Shruti Padmanabha, Andrew Lukefahr, et al. DynaMOS: Dynamic schedule migration for heterogeneous cores. In *MICRO*, 2015.
- [117] Shruti Padmanabha, Andrew Lukefahr, et al. Mirage cores: The illusion of many out-of-order cores using in-order hardware. In *MICRO*, 2017.
- [118] Xulong Tang, Orhan Kislal, et al. Data movement aware computation partitioning. In *MICRO*, 2017.
- [119] Shuang Chen, Yi Jiang, et al. PIMCloud: QoS-Aware Resource Management of Latency-Critical Applications in Clouds with Processing-in-Memory. In *HPCA*, 2022.
- [120] RM Radway, K Sethi, et al. The Future of Hardware Technologies for Computing: N3XT 3D MOSAIC, Illusion Scaleup, Co-Design. In *IEDM*, 2021.
- [121] Konstantinos Kanellopoulos, Konstantinos Sgouras, et al. Virtuoso: Enabling fast and accurate virtual memory research via an imitation-based operating system simulation methodology. In *ASPLOS*, 2025.
- [122] Madhava Sarma Vemuri and Umamaheswara Rao Tida. Efficient and scalable miv-transistor with extended gate in monolithic 3d integration. In *MWSCAS*, 2023.
- [123] Om Prakash, Kai Ni, and Hussam Amrouch. Monolithic 3D integrated BEOL dual-port ferroelectric FET to break the tradeoff between the memory window and the ferroelectric thickness. In *IRPS*, 2023.
- [124] Madhava Sarma Vemuri and Umamaheswara Rao Tida. FDSOI Process Based MIV-transistor Utilization for Standard Cell Designs in Monolithic 3D Integration. In *SOCC*, 2023.
- [125] Kuangye Lu, Jaewoo Shim, et al. 2d materials can unlock single-crystal-based monolithic 3d integration. *Nature Electronics*, 2024.
- [126] Maosong Xie, Yueyang Jia, et al. Monolithic 3D integration of 2D transistors and vertical RRAMs in 1T-4R structure for high-density memory. *Nature Communications*, 2023.
- [127] Shi-Xian Guan, Tilo H Yang, et al. Monolithic 3d integration of back-end compatible 2d material fet on si finfet. *npj 2D Materials and Applications*, 2023.
- [128] Jun-young Kim, Xin Ju, et al. Van der waals layer transfer of 2d materials for monolithic 3d electronic system integration: review and outlook. *ACS nano*, 2023.
- [129] Rahul Pendurthi, Najam U Sakib, et al. Monolithic three-dimensional integration of complementary two-dimensional field-effect transistors. *Nature Nanotechnology*, 2024.
- [130] Yiwei Du, Jianshi Tang, et al. Monolithic 3D integration of FeFET, hybrid CMOS logic and analog RRAM array for energy-efficient reconfigurable computing-in-memory architecture. In *VLSI Technology and Circuits*, 2023.
- [131] Tathagata Srimani, Robert M Radway, et al. Ultra-dense 3d physical design unlocks new architectural design points with large benefits. In *DATE*, 2023.
- [132] Fan Chen, Linghao Song, et al. Marvel: A vertical resistive accelerator for low-power deep learning inference in monolithic 3d. In *DATE*, 2021.
- [133] Ji-Hoon Kang, Heechang Shin, et al. Monolithic 3D integration of 2D materials-based electronics towards ultimate edge computing solutions. *Nature Materials*, 2023.
- [134] Shubham Kumar, Paul R Genssler, et al. Frontiers in AI Acceleration: From Approximate Computing to FeFET Monolithic 3D Integration. In *IFIP/IEEE 31st International Conference on Very Large Scale Integration*, 2023.
- [135] Ye Yu and Niraj K Jha. A monolithic 3d hybrid architecture for energy-efficient computation. *IEEE Tran. on Multi-Scale Computing Systems*, 2018.

- [136] Jiaming Li, Bin Gao, et al. A spatial-designed computing-in-memory architecture based on monolithic 3d integration for high-performance systems. In *NANOARCH*, 2023.
- [137] Yibei Zhang, Yijun Li, et al. 3D stackable CNTFET/RRAM 1T1R array with CNT CMOS peripheral circuits as BEOL buffer macro for monolithic 3D integration with analog RRAM-based computing-in-memory. In *IEDM*, 2023.
- [138] AMD. AMD Accelerating – The High Performance Computing Ecosystem, 2021. <https://www.amd.com/en/events/computex>.
- [139] Amna Shahab, Mingcan Zhu, et al. Farewell My Shared LLC! A Case for Private Die-Stacked DRAM Caches for Servers. In *MICRO*, 2018.